Theory and Experiment of Thin-Film Junction Circulator

H. How, S. A. Oliver, *Member, IEEE,* Stephen W. McKnight, *Member, IEEE,* P. M. Zavracky, *Member, IEEE,* N. E. McGruer, *Member, IEEE,* C. Vittoria, *Fellow, IEEE,* and R. Schmidt

***Abstract*—We have calculated the S-parameters and losses in ferrite–film-junction circulators using a new effective-field theory assuming TEM-like propagation. Conductivity loss dominates the dielectric and magnetic losses in Y-junction circulators fabricated on ferrite films with thicknesses less than 200 μm. It is plausible to fabricate Y-junction thin-film circulator at X-band with insertion loss less than 0.5 dB if the film thickness is larger than 100 μm. The quality of the conductor plane is important in reducing the overall insertion loss of the thin-film-junction circulator.**

I. Introduction

MICROWAVE and millimeter-wave devices and systems are becoming increasingly important for both defense and commercial applications. For example, circulators and phase shifters are the building blocks of high-performance phased-array radars and communications systems. Ferrite reciprocal and nonreciprocal components currently used in transmit/receive (T/R) modules are costly and bulky. The development of monolithic planar ferrite/semiconductor circuits is in great demand. Over the past year, we have applied transferred film technology to the fabrication of monolithic-microwave integrated-circuit (MMIC) devices [1]. This approach avoids the problem intrinsic to the direct film deposition technique by separating the film growth process from the ferrite/semiconductor integration process. In practice, the transferred film approach uses commercially purchased single-crystal yttrium–iron–garnet (YIG) films on nonmagnetic garnet substrates [usually gadolinium–gallium garnet (GGG)], that are then transferred to MMIC semiconductor substrates at temperatures compatible with semiconductor technology.

We have recently transferred single-crystal 100-μm-thick YIG films to metallized silicon substrates and fabricated Y-junction circulators with an integrated two-section microstrip impedance-matching structure [1]. These prototype single-crystal-YIG-film-on-silicon circulators have a bandwidth of 8–12 GHz with a minimum circuit insertion loss of 1.34 dB [1]. Improvements in the magnetic biasing circuit, network matching structure, and ground-plane and external connections are needed. We project that near X-band, the insertion loss for an optimized thin-film circulator will be less than 1 dB for wide-band operation, and less than 0.5 dB for narrow-band operation.

There is now a strong need to theoretically analyze the performance of a thin-film junction circulator. The existing theory [2] is inadequate for film devices since its derivation imposed the following unrealistic assumption: the eddy–current-induced-electromagnetic fields within a ferrite junction is z-independent, where z denotes the coordinate normal to the junction's conductor plane [2]. In this paper, we develop an effective field theory to describe the operation of a thin-film–ferrite-junction circulator. The effective field theory was derived rigorously for a guiding structure supporting TEM-like propagation modes, as occurs for the two-dimensional ferrite-junction circulator assumed by Bosma [3] and by Fay and Comstock [4]. Our new theoretical model takes full account of not only the effective values of the junction geometry, permeability, and permittivity, but also of the dielectric, magnetic, and conductor losses. We find that at X-band, the conductor loss dominates in a Y-junction circulator fabricated on a ferrite film with thickness less than 200 μm. Our calculated S-parameters compare closely with experimental results on a 100-μm-thick YIG circulator.

II. Formulation

A. Effective-Field Theory

We first calculate the eddy–current induced electromagnetic fields within a parallel-plate waveguide structure supporting TEM propagation waves (see Fig. 1). In Fig. 1, the two parallel plates are located at $x = \pm d/2$ and the waveguide is filled with a medium of permittivity ϵ and permeability μ. In the following, we denote the primary TEM waves in capital letters, and the eddy–current induced fields in small letters. We have

$$\underline{\mathbf{E}} = E_o \exp(ik_o z)\underline{\hat{\mathbf{x}}} \tag{1}$$

$$\underline{\mathbf{H}} = H_o \exp(ik_o z)\underline{\hat{\mathbf{y}}} \tag{2}$$

where $k_o = \omega(\epsilon\mu)^{1/2}$ and ω is the angular frequency. The eddy–current induced electric field at the metal surfaces $x = \pm d/2$ is [5]

$$\underline{\mathbf{e}}(x = \pm d/2, z) = (\mu_o\omega/8\pi\sigma)^{1/2}(1-i)(\mp\underline{\hat{\mathbf{x}}}) \times \underline{\mathbf{H}}(z) \tag{3}$$

Manuscript received October 8, 1997; revised April 24, 1998. This work was supported by the Office of Naval Research and Defense Advanced Research Project Agency under DoD FY1966 Multidisciplinary Research Initiative.

H. How is with Electromagnetic Applications, Inc., Boston, MA 02109 USA.

S. A. Oliver and S. W. McKnight are with the Center for Electromagnetic Research, Northeastern University, Boston, MA 02115 USA.

P. M. Zavracky, N. E. McGruer, and C. Vittoria are with the Electrical and Computer Engineering Department, Northeastern University, Boston, MA 02115 USA.

R. Schmidt was with MA/COM, Inc., Burlington, MA 01803 USA. He is now with Barry Industries, Inc., Attleboro, MA 02703 USA.

Publisher Item Identifier S 0018-9480(98)08024-7.

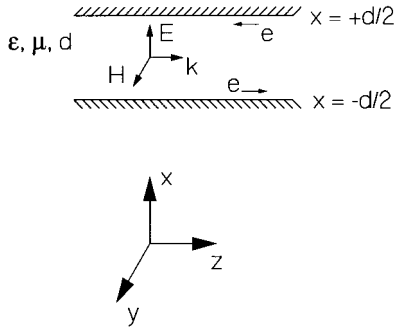

Fig. 1. TEM mode in a parallel-plate waveguide.

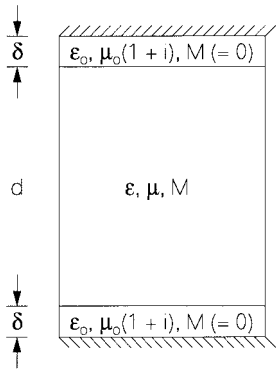

Fig. 2. A circulator junction described as a three-layer structure.

where σ denotes the electrical conductivity of the metal plates. In the waveguide region bounded by the plates, the $\underline{\mathbf{e}}$ field satisfies the following Helmholtz equation:

$$\nabla^2\underline{\mathbf{e}} + k_o^2\underline{\mathbf{e}} = 0 \tag{4}$$

or

$$(\partial^2\underline{\mathbf{e}}/\partial x^2) = 0. \tag{5}$$

This implies

$$\underline{\mathbf{e}}(x,z) = (-2x/d)(\mu_o\omega/8\pi\sigma)^{1/2}(1-i)H_o\exp(ik_oz)\hat{\underline{\mathbf{z}}}, \quad \text{for } |x| < d/2. \tag{6}$$

Note that the eddy–current induced electric field is thus linearly dependent on the vertical distance x, in contrast to the earlier theory [2]. The eddy–current induced magnetic field is

$$\begin{aligned}\underline{\mathbf{h}}(x,z) &= (-ic/\omega\mu)\underline{\nabla}\times\underline{\mathbf{e}}(x,z)\\ &= -(1+i)(\delta/d)(\mu_o/\mu)H_o\exp(ik_oz)\underline{\hat{\mathbf{y}}}\end{aligned} \tag{7}$$

where δ denotes the skin depth of the metal plates

$$\delta = c/\sqrt{2\pi\omega\mu_o\sigma} \tag{8}$$

with c and $\mu_o(=1)$ being the speed of light and the value of permeability in air, respectively. The total field is, therefore,

$$\begin{aligned}\underline{\mathbf{H}}_{\text{tot}}(x,z) &= \underline{\mathbf{H}}(x,z) + \underline{\mathbf{h}}(x,z)\\ &= [1-(1+i)(\delta/d)(\mu_o/\mu)]\underline{\mathbf{H}}(x,z).\end{aligned} \tag{9}$$

In the presence of conductor loss, the guiding structure of parallel plates can no longer support pure-TEM waves since the eddy current will induce an electric field along the propagation direction, given by (6). Furthermore, the conventional wave impedance of the waveguide, defined as the ratio of the transverse electric field to the transverse magnetic field, will be modified as follows:

$$Z_{\text{tot}} = E_o/H_{\text{tot}} = [1-(1+i)(\delta/d)(\mu_o/\mu)]^{-1}(\mu/\epsilon)^{1/2} \tag{10}$$

which gives rise to an effective permeability of the medium

$$\mu_{\text{eff}} = \mu + (2\delta/d)(1+i)\mu_o. \tag{11}$$

By using the effective permeability, the wave impedance of the waveguide can now be written as

$$Z_{\text{tot}} = (\mu_{\text{eff}}/\epsilon)^{1/2} \tag{12}$$

as is done for a conventional medium in the absence of conductor loss.

Therefore, in the presence of conductor loss, the wave impedance of a parallel-plate waveguide will change according to (11), which implies the following geometric interpretation. The effective permeability of the structure is the average value of that containing one layer of the waveguide material of thickness d and two layers of air of thickness δ. However, in addition to the inductor current, the air layers shall be equipped with an equal amount of conductor current responsible for the eddy–current effect. That is, the air layers are described by a permeability

$$\mu_o(1+i).$$

Thus, the conductor loss can be effectively accounted for by withdrawing the metal boundary a distance δ into the interior of the metal with the recessed volume to be filled with an equal amount of conductor and inductor currents. Note that the above picture is analogous to that underlying Wheeler's incremental impedance [6]. We emphasize here that both the effective permeability given by (11) and Wheeler's incremental impedance were derived for a guiding structure supporting TEM-like propagation waves. In addition, the derived effective permeability now shows an explicit dependence on d, the thickness of the waveguide, in contrast to the Neidert's assumption [2].

The effective permeability theory suggests that the parallel-plate waveguide can be described by a composite structure with skindepth layers being filled with air. As such, the inclusion of skindepth layers will also affect the other electromagnetic parameters of the waveguide: the dielectric constant, and the (saturation) magnetization, if a magnetic substance is used as the waveguide medium. This is shown in Fig. 2, where the top and bottom layers are created by the skindepth effect and are described by thickness δ, permittivity ϵ_o, permeability $\mu_o(1+i)$, and magnetization $M=0$. The intermediate layer is the ordinary waveguide material possessing the following parameters of: 1) thickness d; 2) permittivity ϵ; 3) permeability μ; and 4) magnetization M. To be valid in first order, we expect that the overall electromagnetic parameters of the structure can be described as geometric averages of their respective values, as suggested by the effective permeability theory

$$\epsilon_{\text{eff}} = (\epsilon d + 2\epsilon_o\delta)/(d+2\delta) \tag{13}$$

$$\mu_{\text{eff}} = [\mu d + 2\mu_o(1+i)\delta]/(d+2\delta) \tag{14}$$

$$M_{\text{eff}} = Md/(d+2\delta). \tag{15}$$

Note that (14) reduces to (11) if $d \gg \delta$. Thus, this effective-field theory, or mean-field theory, will dictate appreciable difference in the electromagnetic properties when the waveguide thickness d has a magnitude of the order of the skindepth δ, as opposed to large waveguide spacings. We note that in the above derivation, we have assumed the skindepth thickness δ is much smaller than the thickness of metal conductors, denoted as t. In reality, δ can be in the same order of t and, as such, the effective value of δ should be used, which is related to δ and t as follows [7]:

$$\delta_{\text{eff}} = \delta \tanh(d/\delta). \tag{16}$$

Furthermore, the other loss mechanisms can be readily included in the above effective-field theory. The dielectric loss can be included in (13) if the waveguide medium is described by a complex permittivity value [8]

$$\epsilon = \epsilon_r \epsilon_o (1 + i \tan \delta_d) \tag{17}$$

where ϵ_r is the dielectric constant of the waveguide material and $\tan \delta_d$ is its dielectric loss tangent. The magnetic loss in a saturated ferrite medium can be accounted for if the internal dc bias magnetic field H_i is modified to

$$H_i' = H_i - (i\Delta H/2)(f/f_r) \tag{18}$$

where ΔH is the ferromagnetic resonance (FMR) linewidth measured at frequency f_r. The ferrite medium is then described by the Polder permeability tensor [8]

$$\underline{\mu} = \begin{pmatrix} \mu & i\kappa & 0 \\ -i\kappa & \mu & 0 \\ 0 & 0 & 1 \end{pmatrix} \tag{19}$$

where μ and κ are given as

$$\mu = 1 + \frac{f_o f_m}{f_o^2 - f^2} \quad \kappa = \frac{f f_m}{f_o^2 - f^2} \tag{20}$$

and f is the frequency and f_m and f_o are defined as

$$f_m = 4\pi\gamma M_s \tag{21}$$

$$f_o = \gamma H_i'. \tag{22}$$

Here, γ is the gyromagnetic ratio ($\gamma = 2800$ GHz/Oe), $4\pi M_s$ is the saturation magnetization and, in expressing (18), we have assumed the magnetic field to be applied along the z-axis normal to the junction plane. For a single-crystal material, the internal field shall also include the anisotropy field along the z-direction assumed to be coincided with a crystalline symmetry axis.

For a demagnetized ferrite medium, magnetic loss may be distinguished in two cases. For a polycrystalline sample, magnetic domains are randomly oriented. As such, the medium can be described by an isotropic permeability μ, as originally proposed by Schloemann [10]. When magnetic loss is present, we have modified Schloemann's permeability value as follows:

$$\mu = \frac{1}{3} + \frac{2}{3}\left\{\left[1 + \frac{4\pi\gamma M_s}{f(1 - i\gamma\Delta H/2f_r)}\right] \times \left[1 + \frac{-4\pi\gamma M_s}{f(1 + i\gamma\Delta H/2f_r)}\right]\right\}^{1/2}. \tag{23}$$

However, for single-crystal thin-film materials, the direction normal to the film can be an easy direction, for example, YIG grown in a $\langle 111 \rangle$ direction. As such, magnetization of domains in the demagnetized state shall be all parallel/antiparallel to the z-axis, where z denotes the direction normal to the film plane. For this case, we anticipate the following expression for the permeability:

$$\mu = 1 + \frac{4\pi M_s(-if\Delta H/2f_r + 4\pi M_s)}{-(f\Delta H/2f_r)^2 + 4\pi M_s(-if\Delta H/2f_r) - (f/\gamma)^2}. \tag{24}$$

In the past, we have fabricated a Y-junction circulator connected to microstrip feeder lines on a single-crystal YIG-film substrate [1]. The YIG film was of a 100-μm thickness grown along the $\langle 111 \rangle$ direction. While the formulation of a lossy ferrite junction is presented in Section II-B, we have used (24) in describing the lossy behavior of the transmission lines feeding the junction, as will be discussed shortly.

B. Lossy-Ferrite Circulator Junction

We expect that the aforementioned effective-field theory can be applied to a circulator junction since the circulator operation has been explained by Bosma [3] and by Fay and Comstock [4], as resulting from TEM-like precessional modes possessing a Voigt permeability

$$\mu_v = \mu - \kappa^2/\mu \tag{25}$$

where μ and κ are Polder tensor elements given by (20). That is, the circulation modes coincide with Voigt modes, which are guided between the two conductor planes of the junction, forming standing modes for clockwise and counterclockwise rotations. Therefore, by using (13)–(15) with the dielectric constant given by (17) and internal field by (18), not only conductor loss, dielectric loss, and magnetic loss can be taken into account, but also the effective saturation magnetization of the junction can be adequately addressed.

The other two parameters of a circulator junction worth mentioning are the effective junction diameter and its aspect ratio for demagnetization. A ferrite junction is normally formulated by using a cavity model with a magnetic-wall boundary appearing at the periphery of the junction [3], [4]. To properly account for the fringing/stray fields at the junction boundary, it is necessary to increase the junction radius R to an effective value [11] of

$$R_c = R + (d/\pi)[\ln(\pi R/2d) + 1.7726] \tag{26}$$

where d denotes the thickness of the ferrite medium in the junction. For a ferrite puck, one may relate the internal field H_i with the externally imposed field H_o by the following equation:

$$H_i = H_o - N_z 4\pi M_s \tag{27}$$

where N_z denotes the axial demagnetization factor of the ferrite puck, which, when approximated as an ellipsoid, yields the following expression [8]:

$$N_z = (1 + e^2)(e - \tan^{-1} e)/e^3. \tag{28}$$

Here, e denotes the eccentricity of the ellipsoid given by

$$e = (4R^2 - d^2)/d. \tag{29}$$

However, if the same ferrite is used as the dielectric filling material for the circulator junction, e.g., in Wu and Rosenbaum's design [12], $N_z = 1$.

To complete the formulation of this paper, we summarize in the following the expressions required for solving a $3N$-port circulator junction [8]. For a $3N$-port circulator junction, we denote port 1 as the incident port; port $1+N$ and port $1+2N$ are through ports connected with matched loads, and the other ports are open-circuit ports (tuning ports). The jth port $1 \le j \le 3N$ is centered at $\phi = \phi_j$ with a suspension angle $2\theta_j$. In order for circulation action to occur, the junction must exhibit threefold symmetry. The interport impedance of the circulator is

$$G_{ij} = -iZ_f\left(\frac{\theta_j}{\pi}\right)\sum_{n=-\infty}^{\infty}\left[\frac{n}{x}\left(1+\frac{\kappa}{\mu}\right) - \frac{J_{n+1}(x)}{J_n(x)}\right]^{-1} \times\left(\frac{\sin n\theta_i}{n\theta_i}\right)\left(\frac{\sin n\theta_j}{n\theta_j}\right)e^{in(\phi_i-\phi_j)} \tag{30}$$

where x and Z_f are defined as

$$x = k_v R \quad Z_f = (\mu_v\mu_o/\epsilon_f\epsilon_o)^{1/2} \tag{31}$$

and k_v is the wave propagation constant of Voigt modes given by

$$k_v = (\epsilon_f\mu_v)^{1/2}\omega/c \tag{32}$$

and μ_v is the Voigt permeability defined in (25). Let the incident RF magnetic field at port 1 be $h_\phi^{(o)}$. We denote the amplitude of h_ϕ in port j as a_j, $1 \le j \le 3N$. We then have

$$\sum_{j=1}^{3N}(Z_i\delta_{ij} + G_{ij})a_j = 2Z_d h_\phi^{(o)}\delta_{i1} \tag{33}$$

where Z_j denote the wave impedance of port j and

$$\begin{aligned} Z_j &= Z_d, \qquad \text{if } j = 1, 1+N, 1+2N \\ &= iZ_d\cot(x_j\omega\sqrt{\epsilon_{\rm re}})/c, \qquad \text{otherwise.} \end{aligned} \tag{34}$$

Here, x_j is the length of the open-circuited port j, Z_d is defined as

$$Z_d = (\mu_o/\epsilon_d\epsilon_o)^{1/2} \tag{35}$$

and ϵ_d is the dielectric constant of the feeder-line material. In (34), $\epsilon_{\rm re}$ denotes the effective relative dielectric constant of the jth port. For stripline ports $\epsilon_{\rm re} = \epsilon_d$, and for microstrip ports $\epsilon_{\rm re} = 1 + q(\epsilon_d - 1)$, where q denotes the filling factor of the dielectric in the microstrip transmission lines.

Thus, the RF field at the through ports can be solved from (33), which give rise to the following scattering parameters:

$$\begin{aligned} S_{11} &= 1 - a_1/h_\phi^{(o)} \\ S_{(1+N)1} &= -a_{1+N}/h_\phi^{(o)} \\ S_{(1+2N)1} &= -a_{1+2N}/h_\phi^{(o)}. \end{aligned} \tag{36}$$

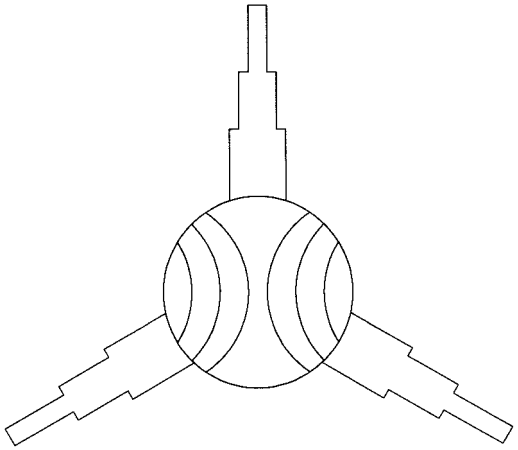

Fig. 3. A circulator junction fed by three three-section impedance-matching transformers.

Before ending this section, we would like to mention a very important numerical technique in solving the junction interport impedance, shown in (30). In (30), we have purposely arranged Bessel functions appearing in ratios involving successive orders. In a lossless case, one can easily evaluate Bessel functions using conventional routines incorporating (Chebyshev) polynomial interpolation and iteration. However, for a lossy junction, Bessel functions having complex arguments must be evaluated, and, hence, the conventional routines are not applicable. Instead, we suggest a method to evaluate ratios of Bessel functions by using the following algorithm involving continued fractions [13]:

$$\frac{J_v(z)}{J_{v-1}(z)} = \frac{1}{2(v+1)z^{-1}} - \frac{1}{2(v+1)z^{-1}} - \frac{1}{2(v+2)z^{-1}} - \cdots \tag{37}$$

where z can be a complex number and v a real number (not necessarily an integer). Equation (37) converges very rapidly and the radii of convergence in the z-plane and v-axis are both infinite. For positive integer n no larger than 20, and for a real positive x smaller than 100, the above expression, which evaluates $J_n(x)/J_{n+1}(x)$ to an accuracy of 10^{-15}, requires less than 25 terms. For larger n, more terms are needed, and for $n = 100$ about 45 terms are required to achieve an accuracy of 10^{-15}.

C. Feeder-Line Network Transformer

Fig. 3 shows a circulator junction with RF magnetic lines shown on the junction responding to circulation operation. A top view of the microstrip impedance-matching network is also shown in Fig. 3, consisting of three three-section transformers. The equivalent circuit model of Fig. 3 is shown in Fig. 4. In Fig. 4, the junction is represented by a 3×3 scattering matrix $(\underline{\underline{\mathbf{S}}})_{3\times3}$, and each of the transformers is represented by a 2×2 scattering matrix $(\underline{\underline{\mathbf{T}}})_{2\times2}$. The scattering matrix $\underline{\underline{\mathbf{S}}}$ can be calculated using (34), and has the following form:

$$\underline{\underline{\mathbf{S}}} = \begin{pmatrix} S_{11} & S_{1(1+2N)} & S_{1(1+N)} \\ S_{1(1+N)} & S_{11} & S_{1(1+2N)} \\ S_{1(1+2N)} & S_{1(1+N)} & S_{11} \end{pmatrix}. \tag{38}$$

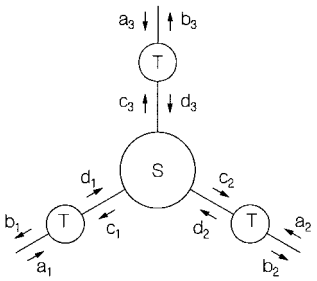

Fig. 4. Equivalent circuit of Fig. 3 showing the scattering matrices $\underline{\underline{\mathbf{S}}}$ and $\underline{\underline{\mathbf{T}}}$ together with propagation waves.

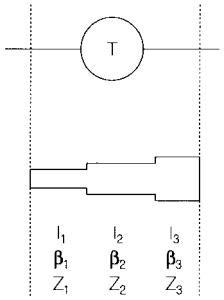

Fig. 5. The scattering matrix corresponding to the impedance-matching transform shown in Fig. 4.

From Fig. 4, we have

$$\underline{\mathbf{c}} = \underline{\underline{\mathbf{S}}}\,\underline{\mathbf{d}} \tag{39}$$

$$\underline{\mathbf{b}} = T_{11}\underline{\mathbf{a}} + T_{12}\underline{\mathbf{c}} \tag{40}$$

$$\underline{\mathbf{d}} = T_{21}\underline{\mathbf{a}} + T_{22}\underline{\mathbf{c}}. \tag{41}$$

The overall scattering matrix $\underline{\underline{\mathbf{W}}}$ is defined as

$$\underline{\mathbf{b}} = \underline{\underline{\mathbf{W}}}\,\underline{\mathbf{a}} \tag{42}$$

which can then be solved as

$$\underline{\underline{\mathbf{W}}} = T_{11}\underline{\underline{\mathbf{I}}} + T_{12}T_{21}\underline{\underline{\mathbf{S}}}(\underline{\underline{\mathbf{I}}} - T_{22}\underline{\underline{\mathbf{S}}})^{-1}. \tag{43}$$

The remaining task is to formulate the scattering matrix $\underline{\underline{\mathbf{T}}}$ corresponding to a three-section transformer, as shown in Fig. 5. In Fig. 5, we denote the length, propagation constant, and impedance of the jth section as ℓ_j, k_j, and Z_j, where $1 \le j \le 3$. We assume TEM waves are propagating in these feeder line elements. In Section I, we assume the total RF electric field is

$$\exp(ik_1 z) + T_{11}\exp(-ik_1 z).$$

In Section II, the total RF electric field is

$$\alpha\exp(ik_2 z) + \beta\exp(-ik_2 z)$$

and, in Section III, the total RF electric field is

$$T_{21}\exp(ik_3 z).$$

The boundary conditions require the tangential components of the RF electric and magnetic fields to be continuous across the section boundaries. This implies

$$\exp(ik_1\ell_1) + T_{11}\exp(-ik_1\ell_1) = \alpha\exp(ik_2\ell_1) + \beta\exp(-ik_2\ell_1) \tag{44}$$

$$\alpha\exp[ik_2(\ell_1+\ell_2)] + \beta\exp[-ik_2(\ell_1+\ell_2)] = T_{21}\exp[ik_3(\ell_1+\ell_2)] \tag{45}$$

$$[\exp(ik_1\ell_1) - T_{11}\exp(-ik_1\ell_1)]/Z_1 = [\alpha\exp(ik_2\ell_1) - \beta\exp(-ik_2\ell_1)]/Z_2 \tag{46}$$

$$\{\alpha\exp[ik_2(\ell_1+\ell_2)] - \beta\exp[-ik_2(\ell_1+\ell_2)]\}/Z_2 = T_{21}\exp[ik_3(\ell_1+\ell_2)]/Z_3. \tag{47}$$

Therefore, T_{11} and T_{21} are solved as (48) and (49), shown at the bottom of this page. Similar formulas can be derived for T_{12} and T_{22}, provided that indexes 1 and 3 in (48) and (49) are interchanged, respectively. We note that in the above derivation, the propagation constants k_j, $1 \le j \le 3$ can be a complex number to account for a lossy feeder line. For a lossy microstrip line fabricated on a dielectric substrate, the attenuation constant can be found in [14]. For a microstrip line fabricated on a demagnetized substrate, the necessary formulas can be found in [15], where the duality relationships between electric and magnetic behaviors have been utilized. For a demagnetized ferrite substrate, the permeability value has been given in (23) and (24).

III. Calculational Results

In order to explore the insertion-loss limit of using a thin-film-junction circulator, we have considered the X-band circulator design proposed by Wu and Rosenbaum [12]. We assume a single-crystal YIG thin-film of $\langle 111\rangle$ orientation is used as the junction material, which is fed by the three three-section transformers shown in Fig. 3. The YIG film possesses the following parameters:

1) dielectric constant $\epsilon_d = \epsilon_f = 14.5$;
2) dielectric loss-tangent $\tan\delta = 0.0002$;
3) saturation magnetization $4\pi M_s = 1750$ G;
4) FMR linewidth $\Delta H = 1$ Oe measured at $f_r = 10$ GHz.

The junction is of a radius 2.76 mm, which results in maximal transmission at $f_{\max} = 9.3$ GHz (see Fig. 6). We consider the junction has only three ports (Y-junction) with the port suspension angle $2\theta = 1.0$ rad. The junction is locally biased by a permanent magnet to just saturate the junction $H_i = 0$ Oe. Copper is used as the material for the metal circuit and for the ground plane whose thickness is 2 μm.

$$T_{11} = \frac{(Z_2+Z_1)(Z_2-Z_3)\exp(ik_2\ell_2) - (Z_2-Z_1)(Z_2+Z_3)\exp(-ik_2\ell_2)}{(Z_2-Z_1)(Z_2-Z_3)\exp(ik_2\ell_2) - (Z_2-Z_1)(Z_2+Z_3)\exp(-ik_2\ell_2)}\exp(2ik_1\ell_1) \tag{48}$$

$$T_{21} = \frac{-4Z_2Z_3\exp(ik_1\ell_1)\exp(ik_2\ell_2)}{(Z_2-Z_1)(Z_2-Z_3)\exp(ik_2\ell_2) - (Z_2-Z_1)(Z_2+Z_3)\exp(-ik_2\ell_2)} \tag{49}$$

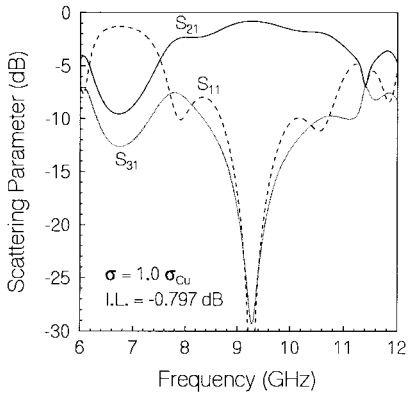

Fig. 6. Calculated scattering parameters of a thin-film Y-junction circulator at X-band. The circulator is adopted from Wu and Rosenbaum's design, and the film thickness is 100 μm.

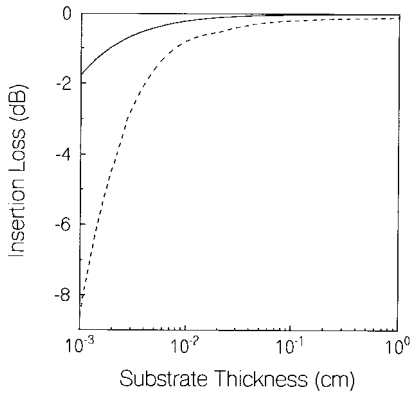

Fig. 7. Calculated insertion loss as a function of the ferrite substrate thickness for a circulator junction (solid line) and for a circulator junction plus a network transformer (dashed line).

We consider the network transformer to consist of three sections. The first section requires the microstrip line to have an impedance $Z_1 = 50\ \Omega$. The impedance of the third microstrip section is fixed by the suspension angle of the junction ports and the thickness of the substrate. The second section serves as a $\lambda/4$ transform, which requires the impedance $Z_2 = (Z_1 Z_3)^{1/2}$. The length of each microstrip section is referred to the wavelength at maximal transmission $f_{\max} = 9.3$ GHz. The length of the second section is required to be one quarter-wavelength at $f_{\max}$. Although there is no restriction on the length of the first and third microstrip sections, we have assumed that they are also of one quarter-wavelength at $f_{\max}$, even though the insertion loss can be further reduced if shorter lines are used. A general discussion on broad-band matching can be found in [16].

Fig. 6 shows the calculated S-parameters of the junction circulator, including the three-section $\lambda/4$ matching network transformer, and assuming the single-crystal YIG substrate is of a thickness 100 μm. The calculated insertion loss at $f_{\max}$ is -0.797 dB, of which -0.208 dB is due to the junction loss, and the remainder is the loss in matching transformers. Magnetic and dielectric losses in the junction are, respectively, $-0.009\,91$ and $-0.006\,82$ dB, both negligibly small with respect to conductor loss in the junction. For comparison, the method of Neidert and Phillips [2] predicts a conductivity loss of -0.09 dB in the junction. We note that the overall insertion loss of the junction plus the network transformers can be lowered to -0.433 dB if the length of the first and third microstrip sections are reduced to one-tenth of the wavelength at $f_{\max}$.

Fig. 7 plots the calculated insertion loss as a function of the ferrite substrate thickness. The solid line represent the insertion loss due to the junction alone, whereas the dashed line refers to the total loss of the junction, plus the transformer network. We note that when the substrate thickness decreases below 100 μm, not only does the insertion loss increase drastically, as shown in Fig. 7, but also the bandwidth of transmission narrows rapidly as a result of matching the lower junction impedance value to that of 50-Ω feeder lines.

In order to isolate the transformer functions, we have plotted in Fig. 8 the scattering parameters associated with an ideal

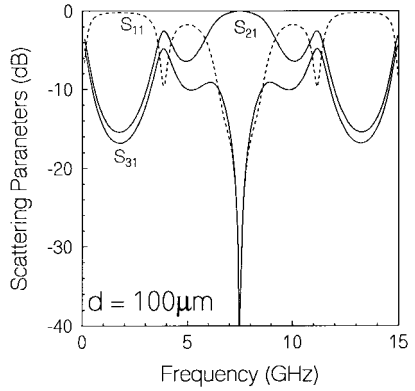

Fig. 8. Calculated scattering parameters of an ideal circulator junction fed by $\lambda/4$ transformers. The ferrite thickness is 100 μm.

circulator junction fed by three three-section transformers. An ideal circulator junction means infinite bandwidth with zero insertion loss and infinite isolation. The transformers are built in a substrate of 100-μm thickness, and we have assumed the transmission lines are all lossless. Thus, Fig. 8 directly reveals the bandwidth information on the employed transformers. From Fig. 8, we conclude that for a thin-film substrate with thickness $d = 100$ μm, a $\lambda/4$ transformer network is not enough to bring about the wide transmission-band feature of a Wu and Rosenbaum's circulator design. More transformer sections are apparently needed to enlarge the transmission bandwidth. Fig. 8 should be compared with Fig. 6 to infer the lossy behavior of the circulator junction plus the transformer networks. A discussion on the loss characteristics of thin-film circulators can be found in [17].

IV. Measurements

We have implemented the transferred-film method to produce a single-crystal YIG film circulator [1]. The transferred-film method involves bonding, at low temperature, thick single-crystal ferrite films to metallized semiconductor dice, removing the ferrite native substrate, and then fabricating the passive microwave circuit using standard semiconductor metallization, photolithography, and etching techniques.

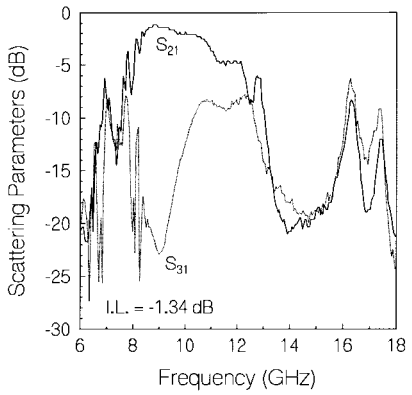

Fig. 9. Measured S_{11} and S_{21} data reported in [1].

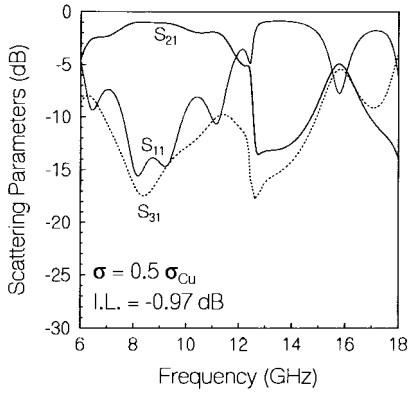

Fig. 10. Calculated scattering parameters of the circulator whose measured S_{11} and S_{21} data are shown in Fig. 9.

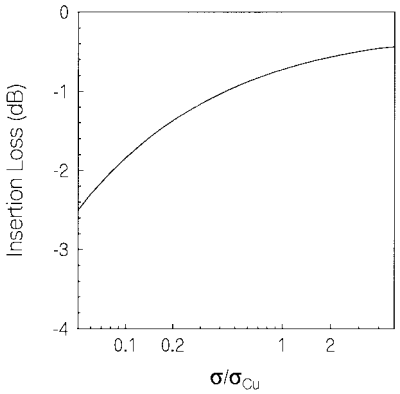

Fig. 11. Calculated insertion loss of the thin-film circulator as a function of metal conductivity.

This method appears to be fully compatible with current wafer–scale batch processing practices.

An X-band Y-junction circulator was fabricated using this technique [1]. The ferrite source material was 100-μm-thick single-crystal (111) YIG film, grown by liquid phase epitaxy onto a GGG substrate. Working at a 0.5 in $\times$ 0.4 in die level, chips of YIG/GGG had a 2-μm-thick copper microwave ground plane deposited onto them, and were then bonded at temperatures below 200 °C to a metallized silicon chip. The GGG native substrate was then removed from the bonded chip by mechanical grinding. The exposed YIG surface was polished, and then metallized by a 2-μm-thick copper film. The circulator circuit was then fabricated using photolithography and etching of the copper film.

The circulator circuit was based on a standard Wu and Rosenbaum design [12] with some modifications. One modification was the use of a two-section transformer to match the resonator input impedance to the 50-Ω SMA[1]-to-microstrip connectors. This design is identical to that shown in Fig. 3, except that the third section is omitted. The junction and transformers are characterized by the following parameters:

1) dielectric constant $\epsilon_d = \epsilon_f = 14.5$;
2) dielectric loss-tangent $\tan\delta = 0.0002$;
3) saturation magnetization $4\pi M_s = 1750$ G;
4) FMR linewidth $\Delta H = 1$ Oe measured at $f_r = 10$ GHz.

The junction is of a radius of 2.49 mm. The length and width of the first microstrip section in the transformer network is $\ell_1 = 2.54$ mm and $w_1 = 0.2$ mm, respectively, and those of the second sections are $\ell_2 = 2.14$ mm and $w_2 = 1.02$ mm, respectively. The internal magnetic field in the resonator was of order 300 Oe.

Fig. 9 shows the measured scattering parameters for the fabricated circuit and connectors using a vector network analyzer [1]. The lowest measured insertion loss (1.34 dB) and highest isolation ($-$20 dB) occur in a 1-GHz band centered at 9.0 GHz. The calculated circulator performance, including both effects from the ferrite junction and from the network transformer, is shown in Fig. 10. In deriving Fig. 10, we have assumed the electric conductivity of the metal circuit and the ground plane is half that of copper $\sigma = 0.5\sigma_{\rm Cu}$. This accounts for the possible degradation of the copper ground-plane conductivity during the bonding process. In Fig. 10, the calculated insertion loss is -0.97 dB, which is about 0.3 dB lower than the measured value. We attribute from 0.2 to 0.3 dB of this difference to loss or reflections from the connectors. Finally, we would like to mention that the insertion loss heavily depends on the metal conductivity. This is shown in Fig. 11, where the calculated insertion loss is plotted as a function of the metal conductivity (normalized with respect to the bulk value of 5.5×10^7 mho/m for copper). From Fig. 11, the calculated insertion loss is -0.74 dB when $\sigma = \sigma_{\rm Cu}$, and it increases to -1.85 dB when $\sigma = 0.1\sigma_{\rm Cu}$. Therefore, it is of crucial importance to produce high-quality metal patches and ground planes in the fabrication of thick-film electronic semiconductor/ferrite circuits.

We should also note that larger insertion losses were measured or calculated in Figs. 9 and 10 than for the design of Fig. 6. The reason for this is that the circulator circuit design used during device fabrication does not operate at the exact circulation condition even if all of the loss mechanisms are turned off. Due to the omission of the third section in the network transformer, the port suspension angle is $2\theta = 0.404$ rad, which is quite different from that required by the circulation condition $(2\theta = 1.0)$. Comparing Fig. 10 with Fig. 9, we notice the calculated scattering parameters exhibit wider bandwidth, and differences outside of the transmission band are also observed. We attribute this discrepancy to

[1] M/A-COM Omni Spectra, Inc., Lowell, MA.

the nonuniform magnetic bias field applied to the circulator junction. The nonuniform magnetic bias field has a pronounced effect in shrinking the transmission bandwidth, as previously detailed by Schloemann and Blight [18], who have pointed out that the original 1:2 bandwidth of Wu and Rosenbaum's circulator design [12] can be increased to a 1:3 bandwidth if the bias field can be made uniform by applying two semi-spherical ferrite radomes [18]. We have investigated this nonuniform field effect by numerically integrated Maxwell equations within the ferrite junction using the implicit fourth-order Runge–Kutta method [19], assuming the same boundary conditions proposed by Bosma [3]. Our calculations clearly indicate the transition from Wu and Rosenbaum's measurements to Schloemann and Blight's measurements as the nonuniformity in bias magnetic field at the edge of the junction increases beyond a threshold value [19]. In addition, we have identified the glitches measured in Fig. 9. They are associated with excitation of a spin–wave manifold in the presence of a nonuniform bias magnetic field at the edge of the ferrite junction [19].

V. Conclusion

We have formulated the operation of a thin-film-junction circulator together with a network transformer. This formulation was based on an effective-field theory, which not only readily accounts for the dielectric loss, magnetic loss, and conductor loss, but also addresses the effective magnetization value of the junction. The theory has been applied to an existing thin-film circulator design to investigate the dependence on the film thickness and metal conductivity. At X-band, it is plausible to fabricate a thin-film circulator with insertion loss less than 0.5 dB, provided the film thickness is larger than 100 μm. This critical film-thickness value scales inversely with the square root of the frequency. It is also of crucial importance to fabricate high-quality metal surfaces to ensure low insertion loss. Our calculations closely compared with measurements.

References

[1] S. A. Oliver, P. M. Zavracky, N. E. McGruer, and R. Schmidt, "A monolithic single crystal yttrium–iron–garnet/silicon X-band circulator," *IEEE Microwave Guided Wave Lett.*, vol. 4, pp. 239–241, Aug. 1997.

[2] R. E. Neidert and P. M. Philips, "Losses in Y-junction stripline and microstrip ferrite circulators," *IEEE Trans. Microwave Theory Tech.*, vol. 41, pp. 1081–1086, June/July 1993.

[3] H. Bosma, "On stripline Y-circulation at UHF," *IEEE Trans. Microwave Theory Tech.*, vol. MTT-12, pp. 61–73, Jan. 1964.

[4] C. E. Fay and R. L. Comstock, "Operation of the ferrite junction circulator," *IEEE Trans. Microwave Theory Tech.*, vol. MTT-13, pp. 15–27, Jan. 1965.

[5] J. D. Jackson, *Classical Electrodynamics*. New York: Wiley, 1975.

[6] H. A. Wheeler, "Formulas for the skin effect," *Proc. IRE*, vol. 30, pp. 412–430, Sept. 1942.

[7] H. How, R. Seed, C. Vittoria, D. B. Chrisey, J. S. Horwitz, C. Carosella, and V. Folen, "Microwave characteristics of high T_c superconducting coplanar waveguide resonator," *IEEE Trans. Microwave Theory Tech.*, vol. 40, pp. 1668–1673, Aug. 1992.

[8] H. How, T.-M. Fang, R. Schmidt, and C. Vittoria, "Design of six-port stripline ferrite junction circulators," *IEEE Trans. Microwave Theory Tech.*, vol. 42, pp. 1272–1275, July 1994.

[9] B. Lax and K. J. Button, *Microwave Ferrites and Ferrimagnetics*. New York: McGraw-Hill, 1962.

[10] E. Schloemann, "Microwave behavior of partially magnetized ferrites," *J. Appl. Phys.*, vol. 41, pp. 204–214, Jan. 1970.

[11] L. C. Shen, "Resonant frequency of a circular disc printed-circuit board," *IEEE Trans. Antenna Propagat.*, vol. AP-25, pp. 596596, July 1977.

[12] Y. S. Wu and F. J. Rosenbaum, "Wide-band operation of microstrip circulators," *IEEE Trans. Microwave Theory Tech.*, vol. MTT-22, pp. 849–856, Oct. 1974.

[13] M. Abramowitz and I. A. Stegun, Eds., *Handbook of Mathematical Functions with Formulas, Graphs, and Mathematical Tables* (Applied Mathematics Series 55). Washington, D.C.: NBS, 1964, p. 363.

[14] R. A. Pucel, D. J. Massé, and C. P. Hartwig, "Losses in microstrip," *IEEE Trans. Microwave Theory Tech.*, vol. MTT-16, pp. 342–350, June 1968.

[15] D. J. Massé and R. A. Pucel, "Microstrip propagation on magnetic substrates—Part II: Experiment," *IEEE Trans. Microwave Theory Tech.*, vol. MTT-20, pp. 309–313, May 1972.

[16] E. Schloemann and R. E. Blight, "A compact broad-band microstrip circulator for phased array antenna modules," in *IEEE MTT-S Microwave Symp. Dig.*, vol. 3, Albuquerque, NM, 1992, pp. 1389–1392.

[17] J. D. Adam, H. Buhay, M. R. Daniel, M. C. Driver, G. W. Eldridge, M. H. Hanes, and R. L. Messham, "Monolithic integration of an X-band circulator with GaAs MMIC's," *IEEE MTT-S Microwave Symp. Dig.*, vol. 1, Orlando, FL, May 14–19, 1995, pp. 97–98.

[18] E. Schloemann and R. E. Blight, "Broad-band stripline circulators based on YIG and Li-ferrite single crystals," *IEEE Trans. Microwave Theory Tech.*, vol. MTT-34, pp. 1394–1400, Dec. 1986.

[19] H. How, S. W. McKnight, S. A. Oliver, P. M. Zavracky, N. E. McGruer, and C. Vittoria, "Influence of non-uniform magnetic field on a ferrite junction circulator," to be published.

H. How, photograph and biography not available at the time of publication.

S. A. Oliver (M'97), photograph and biography not available at the time of publication.

Stephen W. McKnight (M'88) received the B.A. degree in physics from Oberlin College, Oberlin, OH, in 1969, and the Ph.D. degree in solid-state physics from the University of Maryland at College Park, in 1977.

After a research appointment at Emory University, and a National Research Council Fellowship at the Naval Research Laboratory, he joined the faculty of the Physics Department, Northeastern University, Boston, MA, in 1980. He took an appointment in the Center for Electromagnetics Research, an NSF-sponsored Industry/University Collaborative Research Center, in 1985. In 1987, he was appointed Associate Professor in the Department of Electrical and Computer Engineering, Northeastern. Since 1992, he has been an Associate Director of the Center for Electromagnetics Research, Northeastern. He has published over 35 refereed publications on microwave, far-infrared, and optical materials and devices.

Dr. McKnight is a member of the American Physical Society and the IEEE Magnetics Society and IEEE Microwave Theory and Techniques Society.

P. M. Zavracky (M'82–SM'97), photograph and biography not available at the time of publication.

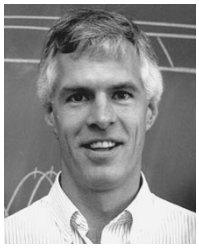

N. E. McGruer (S'83–M'83) currently conducts research in the areas of microelectromechanical systems (MEMS), three-dimensional (3-D) microelectronics, and microfabricated ferrite devices at Northeastern University, Boston, MA. He has also conducted a variety of microfabrication-related research projects, including plasma-source ion implantation for semiconductor doping in multiple-process systems, fabrication of 0.1–2-μm-scale gated field emission devices, gated field emitter reliability physics, fabrication of microrelays and MEM sensors, fabrication of 3-D microelectronic circuits, and fabrication of monolithic ferrite devices. To perform this work, he directs the Scanning Electron Microscopy Facility, and co-directs the Microfabrication Laboratory. From 1983 to 1987, at Sperry Semiconductor Operations, he was responsible for ion implant/diffusion process development for 0.8- and 1.25-μm CMOS technologies, participated in the start-up of a new fabrication facility, and investigated rapid thermal annealing and oxidation of silicon for MOS gate dielectrics.

C. Vittoria (S'62–M'63–SM'83–F'90), photograph and biography not available at the time of publication.

R. Schmidt, photograph and biography not available at the time of publication.